Journal of Molecular Structure 1145 (2017) 102–111

Contents lists available at ScienceDirect

Journal of Molecular Structure

journal homepage: http://www.elsevier.com/locate/molstruc

Synthesis, crystal structure, Hirshfeld surface analysis, electronic structure through DFT study and fluorescence properties of a new anthracene based organic tecton

Nilasish Pal [a, *], Debabrata Singha [a], Atish Dipankar Jana [b, **]

[a] Department of Chemistry, Seth Anandaram Jaipuria College, 10, Raja Nabakrishna Street, Kolkata, 700005, West Bengal, India
[b] Department of Physics, Behala College, Parnashree, Kolkata, 700060, West Bengal, India

ARTICLE INFO

Article history:
Received 28 February 2017
Received in revised form
8 May 2017
Accepted 16 May 2017
Available online 19 May 2017

Keywords:
Anthracene-2-(2′-Pyridyl)imidazole tecton
CH···π interaction
π···π interaction
DFT study
Hirshfeld surface analysis
Fluorescence quenching

InChIKeys:
ICNMPTJGYOSTPH-UHFFFAOYSA-N
RHSQLEZTJXIUCK-UHFFFAOYSA-N
NQRCRSMUMDAGRR-UHFFFAOYSA-N

ABSTRACT

A new organic molecule 9,10-bis((2-(pyridin-2-yl)-1H-imidazol-1-yl)methyl)anthracene (**APIM**) has been synthesized. Crystal structure analysis of the molecular solid reveals that **CH**···π and π···π interactions are the molecular packing forces in the solid state. Thermal analysis of the molecular solid shows relatively higher decomposition temperature of the crystalline molecular solid that correlates well with the cooperative nature of **CH**···π and π···π interactions. Density Functional Theory (DFT) optimized structure of the molecule closely correlates with that found in the crystal. DFT optimizations also lead to the similar **CH**···π and π···π interaction motifs that are found within the crystal. Hirshfeld surface analysis provides detailed insight into the relative importance of various weak forces in the molecular packing. Study of the fluorescence behavior of the molecules shows quenching in the presence of metal ions.

1. Introduction

Designed synthesis of molecular materials with interesting physico-chemical properties is being pursued vigorously throughout the world. In the area of organic molecular materials various weak intermolecular forces such as hydrogen bonding [1–3], π···π interaction [4–7], **CH**···π interaction [8,9] etc., are generally utilized to control the molecular organization in the solid state and to steer properties of the crystalline solid materials [10–13]. At present it has become an art to judiciously combine different functional units into a single molecule to steer the molecular reactivity [14,15], rigidity/flexibility [16–18] and self/mutual interaction [19–21]. This can be done by manipulating various weak forces like hydrogen bonding, aromatic π-stacking interactions etc. In this regard designing molecular units or tectons having desired shape and size with the placement of functional groups at suitable locations on the molecule is the ultimate influencing factors that govern how the molecules unite into super molecules. Through this methodology various supramolecular architectures like molecular rectangle [22,23], molecular cages and containers [24,25] etc. have been designed which are often utilized as nano-scale functional units in nano-devices [26,27].

We report here the design of a new organic molecular tecton based on three different π-stacking units – namely anthracene, pyridine and imidazole. Anthracene moiety posses strong aromaticity and its π-electron system is attractive for the design of luminescent materials [11,28–30]. Pyridyl unit on the other hand is a very versatile one, generally having strong affinity towards metal ions and there are innumerable pyridine based ligands designed with an aim to efficiently bind metal nodes [31,32] producing metal-organic frameworks (MOFs). Imidazole molecule is a biologically important one and is capable of coordination to metal

* Corresponding author.
** Corresponding author.
E-mail addresses: nilasishpal@gmail.com (N. Pal), atishdipankarjana@yahoo.in (A.D. Jana).

http://dx.doi.org/10.1016/j.molstruc.2017.05.074
0022-2860/

center together with hydrogen bonding capability through the –NH group [33–35]. With an aim to combine the above mentioned functionalities simultaneously into a single molecule we have attempted to synthesize a new organic molecular tecton by combining anthracene, pyridine and imidazole groups and have successfully designed a symmetric, semi-rigid and relatively long molecular tecton (Scheme 1). It is expected that the molecular self-assembly of such a molecule should be governed by π-stacking interactions which is indeed the case as revealed by X-ray crystal structure. **CH**···π and π···π interactions cooperatively act in unison resulting supramolecular 2D layers that are stacked inside the solid. A computational study was undertaken to better understand the electronic nature of the molecule and its intermolecular interactions. DFT study reveals that molecule adopts the lowest energy conformation in the solid state and the optimized geometry is in close agreement with the computed one. Geometries of the **CH**···π and π···π motifs have also been computed and the corresponding interaction energies have been estimated. Thermal stability analysis of the crystalline solid reveals a moderately high thermal decomposition temperature correlating with the strong binding of the crystalline solid resulting from cooperative **CH**···π and π···π forces. A fluorescence study has been carried out with a set of metal ions which shows quenching of fluorescence activity in the presence of metal ions.

2. Experimental section

2.1. Material and methods

All solvents and reagents were obtained commercially and used without further purification. Infrared (IR) spectroscopic studies have been carried out with Perkin-Elmer Spectrum one using KBr pellet. ^{1}H NMR and ^{13}C NMR were recorded with Bruker 400 MHz NMR spectrometer. HRMS was recorded on a XEVO-G2QTOF#YA288 spectrometer. Thermal study has been carried out with Perkin Elmer STA 6000 Simultaneous Thermal Analyzer.

2.2. Synthesis of APIM

The desired molecule (**APIM**) has been synthesized easily by the phase transfer catalyst mediated coupling of 2-(2′-Pyridyl)imidazole and 9,10-bis(chloromethyl)anthracene as illustrated in Scheme 1. 2-(2′-Pyridyl)imidazole and 9,10-bis(chloromethyl) anthracene were synthesized in the first stage according to the previously published procedure [36–39].

Next to a solution of 9,10-bis(chloromethyl)anthracene (1 g, 3.63 mmol) and 2-(2′-Pyridyl)imidazole (1.2 g, 7.27 mmol) in chlorobenzene (20 ml), aqueous NaOH (7.5 M, 20 ml) was added. Catalytic amount of tetra butyl ammonium bromide (TBAB) was added to the mixture. The mixture was then refluxed for 6 h. Upon cooling to room temperature a yellow solid precipitate was formed which was collected by filtration and washed with water. The organic layer was washed with water for 2–3 times and dried over Na_2SO_4 and then solvent was removed by rotary evaporator and the combined solid was crystallized from methanol. Good quality light yellow colored crystals suitable for single crystal XRD obtained upon slow evaporation of methanol solution.

^{1}H NMR (400 MHz, $CDCl_3$): δ 8.774 (*dd*, *J* = 4.8 & 0.8 Hz, 1H), 8.452–8.413 (m, 2H), 8.387 (*d*, *J* = 8.0 Hz, 1H), 7.917 (*td*, *J* = 7.6 & 1.6 Hz, 1H), 7.571–7.533 (m, 2H), 7.390–7.357 (m, 1H), 6.967 (s, 2H), 6.958 (*d*, *J* = 1.2 Hz, 1H), 6.431 (*d*, *J* = 1.2 Hz, 1H).

^{13}C NMR (400 MHz, $CDCl_3$): δ 151.29, 148.40, 144.42, 136.99, 131.05, 129.01, 128.33, 126.94, 124.84, 123.14, 122.71, 121.90.

IR (cm^{-1}): 3011 (w), 1673 (m), 1587 (s), 1480 (s), 1453 (s), 1249 (s), 1089 (m), 785 (s), 701 (s).

HRMS (ESI/QTOF) *m/z:* $[M + H]^+$ Calcd for $C_{32}H_{25}N_6$ 493.2141; Found 493.2152.

2.3. X-ray crystallography

Diffraction intensities for the compounds were collected at 293(2) K on a Bruker Kappa Apex-II CCD area-detector diffractometer (MoK_α, λ = 0.71073 Å). The structures were solved by the direct method and refined with full-matrix least-squares technique using the SHELXL-2014 program package [40]. Anisotropic thermal parameters were applied to all the non-hydrogen atoms. The hydrogen atoms were generated using riding atom model. Crystal data as well as details of data collection and refinement for the compound has been summarized in Table 1. Selected bond distances and bond angles are listed in Table 2, π···π interaction data in Table 3 and **C**–**H**···π interaction data in Table 4.

2.4. Hirshfeld surface analysis

Molecular Hirshfeld surfaces [41,42] in the crystal structure are constructed based on the electron distribution calculated as the sum of spherical atom electron densities [43]. For a given crystal structure and set of spherical atomic electron densities, the Hirshfeld surface is unique. The normalized contact distance (d_{norm}) based on both d_e (the distance from the point to the nearest nucleus external to the surface) and d_i (the distance to the nearest nucleus internal to the surface), and the *van der* Waals (*vd*W) radii of the atom, given by equation (1) enables identification of the regions of particular importance to intermolecular interactions [44,45]. The value of the d_{norm} is negative or positive when intermolecular contacts are shorter or longer than *vd*W separations,

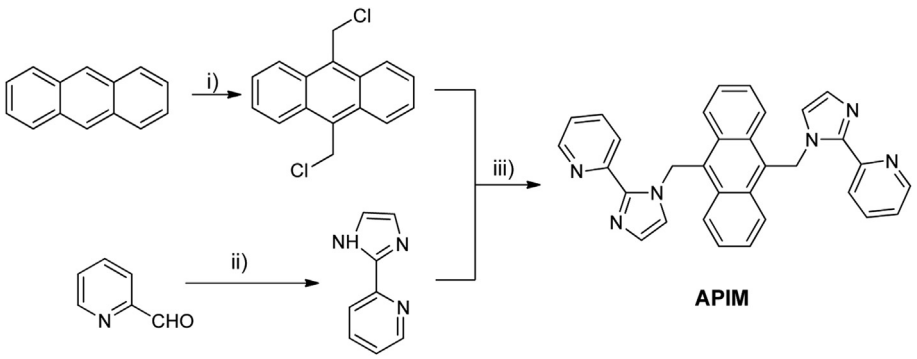

Scheme 1. *Reagent and conditions*: i) Paraformaldehyde, Anh. $ZnCl_2$, Conc. HCl, 1,4-Dioxane ii) 40% Glyoxal, Conc. NH_3, stirring, 1 h, 0 °C, iii) NaOH, PhCl/H_2O, Bu_4NBr, reflux.

Table 1
Crystal data and Refinement parameters.

Crystal Data	
Formula	C_{32} H_{24} N_6
Formula Weight	492.57
Crystal System	triclinic
Space group	$P\bar{1}$ (No. 2)
a, b, c [Å]	7.8590(6) 8.2822(6) 10.0540(8)
alpha, beta, gamma [°]	79.983(4) 72.232(5) 83.858(5)
V [Å^3]	612.68(8)
Z	1
D(calc) [g/cm^3]	1.335
Mu(MoK$_\alpha$) [/mm]	0.082
F(000)	258
Crystal Size [mm]	0.12 × 0.15 x 0.17
Data Collection	
Temperature (K)	293
Radiation [Å]	MoK$_\alpha$ 0.71073
Theta Min-Max [°]	2.5, 27.5
Dataset	−10: 10; −10: 10; −11: 11
Tot., Uniq. Data, R(int)	10648, 2674, 0.041
Observed data [I > 2.0 σ(I)]	2018
Refinement	
Nref, Npar	2674, 172
R, wR_2, S	0.0396, 0.1073, 1.04
Max. and Av. Shift/Error	0.00, 0.00
Min. and Max. Resd. Dens. [e/Å^3]	−0.13, 0.19

w = $1/[\sigma(F_o^2)+(0.0465P)^2+0.0837P]$ where $P=(F_o^2+2F_c^2)/3$.

Table 2
Bond Distance and Bond Angle table (Å, °).

Bond Distances			
N1–C1	1.3669(18)	C6–C7	1.361(2)
N1–C3	1.3721(17)	C7–C8	1.373(2)
N1–C9	1.4728(16)	C9–C10	1.5169(18)
N2–C2	1.369(2)	C10–C11	1.4114(17)
N2–C3	1.3254(17)	C10–C16	1.4068(18)
N3–C4	1.3436(18)	C11–C12	1.4331(19)
N3–C8	1.3363(19)	C11–C16*	1.4428(18)
C1–C2	1.354(2)	C12–C13	1.355(2)
C3–C4	1.4762(19)	C13–C14	1.412(2)
C4–C5	1.387(2)	C14–C15	1.354(2)
C5–C6	1.377(2)	C15–C16*	1.4340(18)
Bond Angles			
C1–N1–C3	106.62(11)	C10–C16–C11*	120.44(11)
C1–N1–C9	123.93(11)	C10–C16–C15*	121.58(12)
C3–N1–C9	128.46(11)	C11*–C16–C15*	117.97(12)
C2–N2–C3	105.20(11)	N1–C1–H1	127
C4–N3–C8	117.48(13)	C2–C1–H1	127
N1–C1–C2	106.36(12)	N2–C2–H2	125
N2–C2–C1	110.75(13)	C1–C2–H2	125
N1–C3–N2	111.07(12)	C4–C5–H5	120
N1–C3–C4	126.50(11)	C6–C5–H5	120
N2–C3–C4	122.41(12)	C5–C6–H6	120
N3–C4–C3	118.49(12)	C7–C6–H6	120
N3–C4–C5	121.62(13)	C6–C7–H7	121
C3–C4–C5	119.84(12)	C8–C7–H7	121
C4–C5–C6	119.14(14)	N3–C8–H8	118
C5–C6–C7	119.68(16)	C7–C8–H8	118
C6–C7–C8	117.97(16)	N1–C9–H9A	109
N3–C8–C7	124.10(15)	N1–C9–H9B	109
N1–C9–C10	113.25(11)	C10–C9–H9A	109
C9–C10–C11	120.53(12)	C10–C9–H9B	109
C9–C10–C16	119.11(11)	H9A–C9–H9B	108
C11–C10–C16	120.28(11)	C11–C12–H12	119
C10–C11–C12	122.95(12)	C13–C12–H12	119
C10–C11–C16*	119.25(12)	C12–C13–H13	120
C12–C11–C16*	117.80(11)	C14–C13–H13	120
C11–C12–C13	121.59(13)	C13–C14–H14	120
C12–C13–C14	120.51(14)	C15–C14–H14	120
C13–C14–C15	120.37(13)	C14–C15–H15	119
C14–C15–C16*	121.61(13)	C16*–C15–H15	119

* = -x,1-y,1-z.

respectively. The combination of d_e and d_i in the form of a two-dimensional (2D) fingerprint plot provides a summary of intermolecular contacts in the crystal [41]. The Hirshfeld surfaces are mapped with d_{norm} and 2D fingerprint plots presented in this paper were generated using Crystal-Explorer 2.1 [46]. Graphical plots of the molecular Hirshfeld surfaces mapped with d_{norm} used a red, white, blue color scheme, where red highlights shorter contacts, white is used for contacts around the *vd*W separation, and blue is for longer contacts. Moreover, two further colored properties (shape index and curvedness) based on the local curvature of the surface can be specified.

$$d_{norm} = \frac{d_i - r_i^{vdw}}{r_i^{vdw}} + \frac{d_e - r_e^{vdw}}{r_e^{vdw}} \quad (1)$$

2.5. Methodology of DFT study

For understanding the stability of the **APIM** molecule and its various π-stacked motifs have been explored through DFT computations. All calculations were performed using the GAUSSIAN package [47]. Initial geometries of the **APIM** molecule and its π-stacked dimeric **C**–**H**···π, π···π motifs were adopted from the crystal structure and geometry optimizations for each one has been carried out at the DFT 6-311G level of theory with B3LYP hybrid density functional. The binding energy for these motifs have estimated according to the formula, B.E. = (Energy of the motif) − 2*(Energy of a single molecule). The torsional rotational barrier potential of the pyridyl ring with respect to the imidazole ring around the imidazole pyriyl C3–C4 bond (Fig. 1) has been computed at the same level of theory.

3. Result and discussion

3.1. X-ray crystal structure

The ORTEP view of **APIM** has been shown in Fig. 1 which shows that imidazolyl-*N* and Pyridyl-*N* are in *trans* geometry on either side of the central anthracene moiety.

The molecule is centrosymmetric with the centre of inversion at the middle of the central phenyl ring of the anthracene moiety. On each side of the central anthracene moiety, two pyridyl imidazole units are attached through C–N bond. The N1–C9–C10 angle is 113.25°. The linear extension of the ligand across two N atoms (N2 and N2*) of two imidazole ring is 11.754 Å. The imidazole ring plane is inclined by 45.18° with respect to the perpendicular plane of the anthracene moiety passing through the C9–C9* axial direction. The farthest hydrogen atom (H) attached to the imidazole ring is at a distance 4.12 Å above and below the anthracene mean plane and the centroid of this ring is 2.09 Å above the anthracene mean plane. The centroid of the pyridyl ring is just 0.75 Å away from the anthracene mean plane. The linear extension of the molecule across the pyridyl ring is 17.99 Å. The dihedral angle between the pyridyl and the imidazole ring plane is 19.13°. Two donor N atoms, N1 and N3 attached respectively to the imidazole ring and the pyridyl ring respectively are rotate by 158.50° with respect to each other.

The supramolecular assembly of the ligand in the solid state is governed by the π-stacking interactions. Molecules assemble into a stacked array along crystallogrphic ***b***-axis by **CH**···π interaction (Table 4). C2 atom of the imidazole ring acts as hydrogen donor to the peripheral phenyl rings of the anthracene moiety. The symmetric nature and step like shape (**Z**-shape) of the molecule is amenable for this self-complementary assembly leading to the formation of molecular rectangle and subsequently to a molecular

Table 3
Geometrical parameters (Å, °) for the face to face π-stacking interactions in the crystalline compound.

Interacting rings	Distance between centroid of R(i) and centroid of R(j) (Å)	Dihedral angle (°)	Slip angle (°)	Perpendicular distance of R(i) centroid from R(j) ring plane (Å)
R1→R1^{i}	3.5355(9)	5.8	5.8	3.5177(6)
R2→ R2^{j}	3.8399(10)	20.4	20.4	−3.5995(6)
i = 1-X,-Y,-Z	**R1:** N1→C1→C2→N2→C3→			
j = 1-X,-Y,1-Z	**R2:** N3→C4→C5→C6→C7→C8→			

Table 4
Geometrical parameters (Å, °) for the edge to face **C**–**H**···π interactions in the crystalline compound.

X-H→ ring(j)	X-H···R(j) angle(°)	Distance between H atom and ring centroid (j) (Å)	X··· centroid ring (j) distance(Å)
C2–H2→ R4^{i}	174	2.63	3.5670(16)
C2–H2→ R4^{ii}	174	−2.63	3.5670(16)
i = X,-1+Y,Z	**R4:** C11→C12→C13→ C14→C15→C16*→		
ii = -X,-Y,1-Z	* = -x,1-y,1-z		

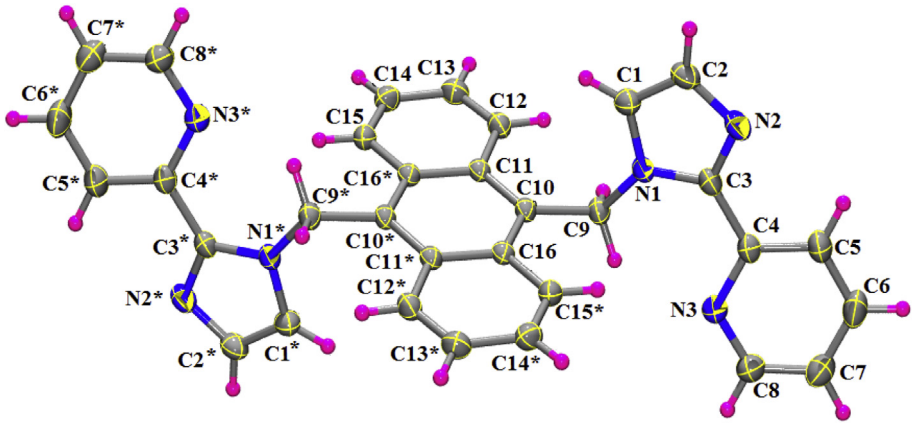

Fig. 1. The ORTEP diagram (30% ellipsoidal probability) with atom numbering scheme. Symmetry equivalent atoms has symmetry code * = -x, 1-y, 1-z.

tape (Fig. 2). Adjacent tapes are joined into a 2D sheet [(**110**) planes] by π···π interaction among the imidazole rings of adjacent tapes. The centroid to centroid distance between the interacting imidazole rings is 3.5355(9) Å (Table 3). Successive (**110**) planes are stacked along ***c***-axis (Fig. 3) through π-stacking interactions involving pyridyl rings (centroid to centroid distance 3.8399(10) Å (Table 3) which protrude out on both sides of the mean plane of (**110**) sheets.

3.2. Hirshfeld surface analysis

Hirshfeld surface analysis has become a popular tool to understand the relative importance of various atom … atom interactions in a crystalline solid. The d_{norm} surface, curvedness and shape index for **APIM** has been depicted in Fig. 4. d_{norm} range is between −0.14 Å to 1.2 Å; shaped index range is −1.0 Å to 1.0 Å and curvedness range is −4.0 Å to 0.4 Å. Two sets of complementary deep red spots (a, a′) and (b,b′) and two relatively lighter red spots (c and d) are clearly visible on the d_{norm} surface. Red regions on the molecule indicate region of contacts on the molecule which are shorter than the *van der* Waal's distances of interacting atoms. Blue regions are at a distance greater than the *van der* Waal's distance and white regions are those where distances are comparable to *van der* Waal's distances. Region marked 'a' is on one of the peripheral rings of anthracene and its complementary region 'a'' is situated on the imidazole group of **APIM**. These two self-complementary regions of **APIM** are responsible for **C**–**H**···π interactions between successive **APIM** molecules that lead to their assembly in the *ab*-plane. 'b' and 'b'' correspond to π···π interaction regions where imidazole groups come in close contact with each other. Intra molecular hydrogen bonding (**CH**···**N**) contact regions are marked by c and d on d_{norm} surface. The curvedness surface shows regions over the molecule are separated from each other by blue boundaries and also correspond to regions which are involved in similar nature of interactions. In the shape index curve blue regions are convex and red regions are concave.

The fingerprint plot has been depicted in Fig. 5. **C···H** interactions and **C···C** interactions contribute respectively 31.7% and 4.2% of total interactions. In the **C···H** fingerprint plot two symmetric broad peaks are visible with $d_i + d_e \succ 3.4$ Å. The **π···π** interactions in the **C···C** fingerprint plot are the broad green region with $d_i + d_e$ in-between 3.4 Å to 4.0 Å. The **C···H** fingerprint plot mainly corresponds to **C**–**H**···π interactions and **C**···**C** fingerprint plot mainly correspond to π···π interactions. As **C**···**H** interactions are overwhelmingly greater than **C**···**C** interactions (31.7% and 4.2% respectively) it can be concluded that **C**–**H**···π interactions play more important role than **π···π** interactions in the crystal. As overall **C**··· all interaction is 39.2%, it is obvious that **CH**···π and π···π are the two main contributors where carbon atoms are involved. The other small (3.3%) share of **C**··· all interaction is between nitrogen atoms and carbon atoms. The overall importance of nitrogen atoms in the molecular interactions is just 14.0%, depicted in the **N**··· all fingerprint plot this shows two sharp spikes corresponding to intra-molecular **CH···N** interaction responsible for

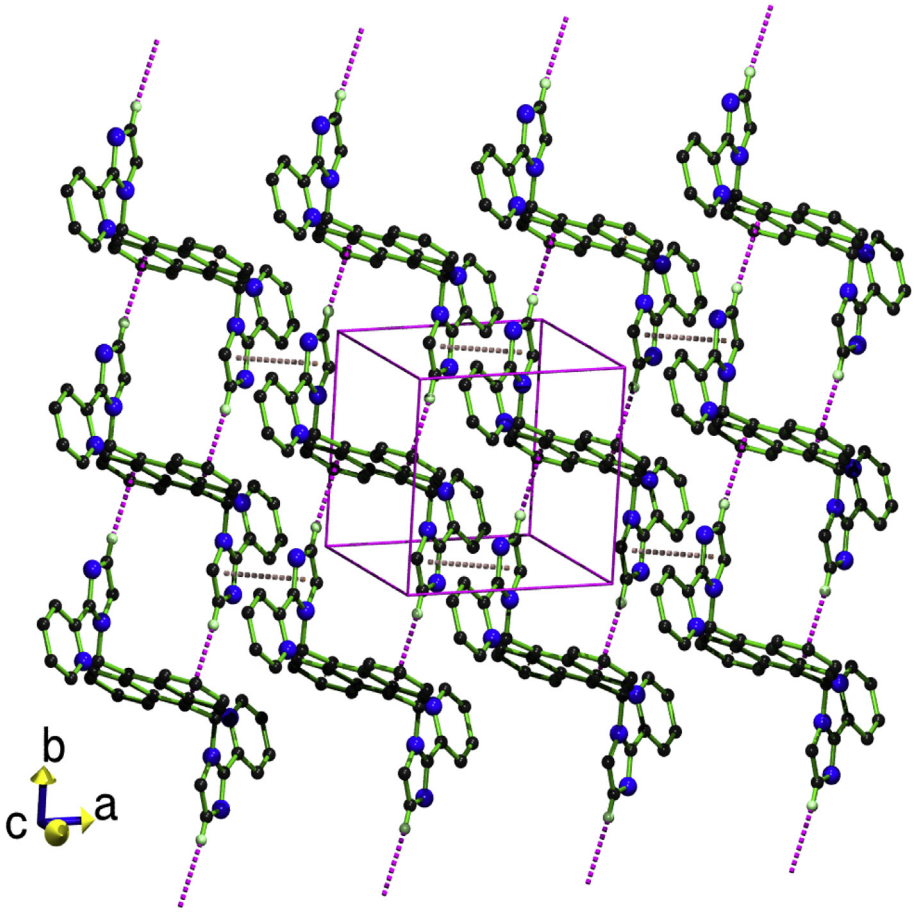

Fig. 2. Supramolecular assembly of the molecules into a 2D sheet through π···π and **C**–**H**···π interaction.

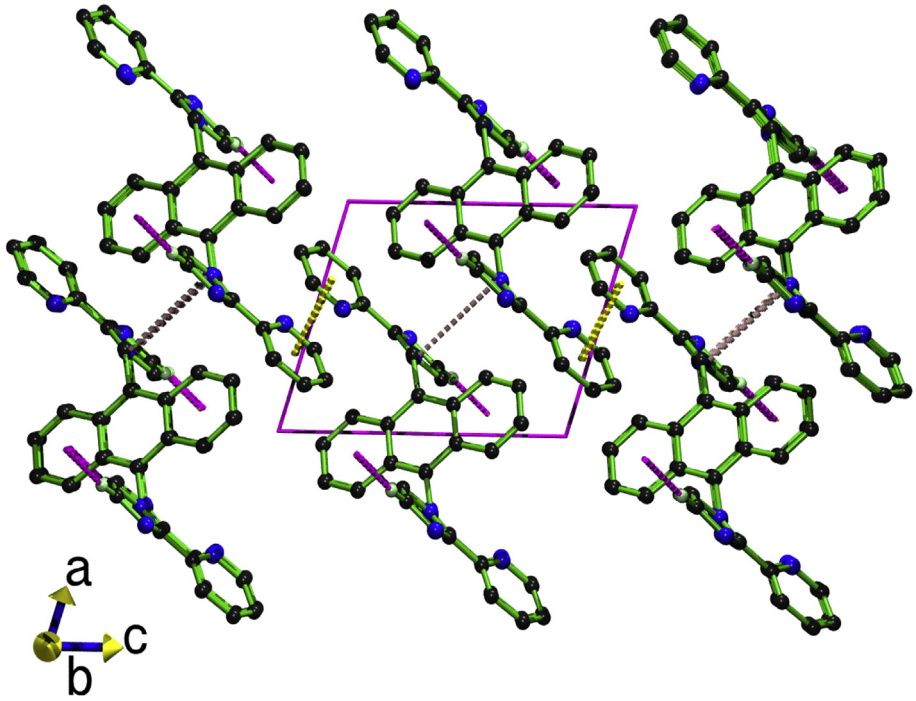

Fig. 3. 3D packing of 2D layers in the crystal.

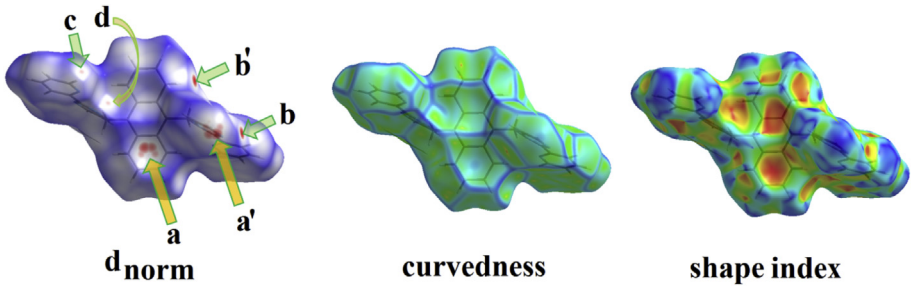

Fig. 4. d_{norm}, curvedness and shape index surfaces of **APIM**.

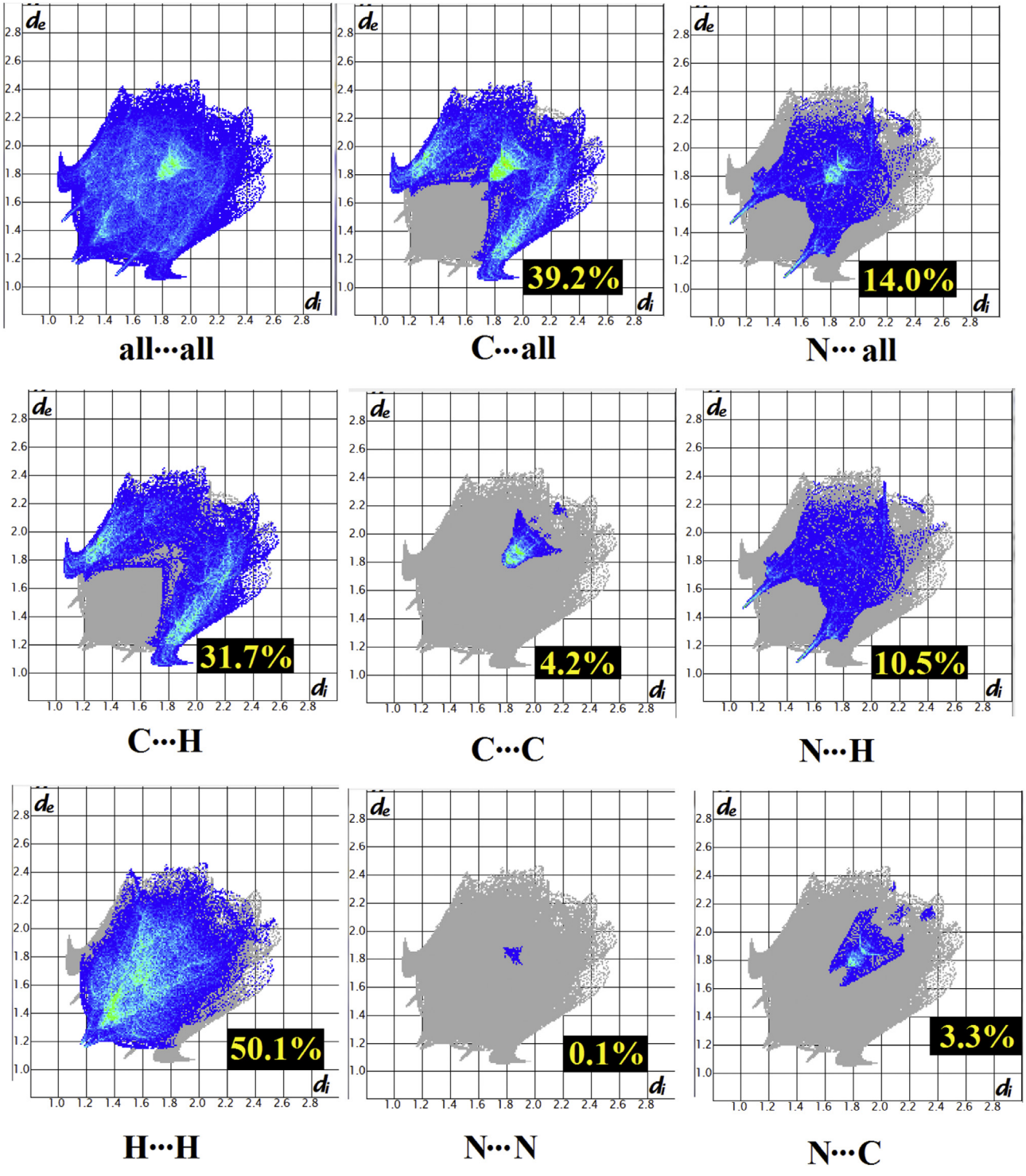

Fig. 5. Finger print plot of intermolecular interactions present in the crystal of compound **APIM**.

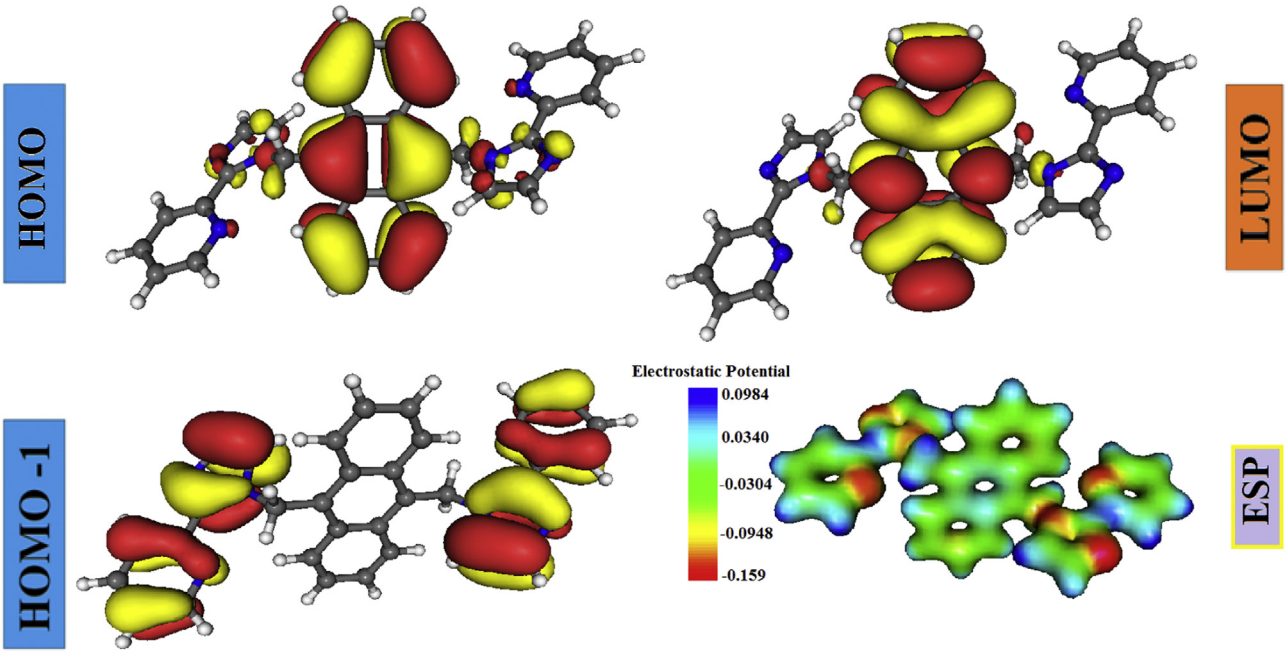

Fig. 6. HOMO, LUMO, HOMO -1and electrostatic potential(ESP) surface of APIM.

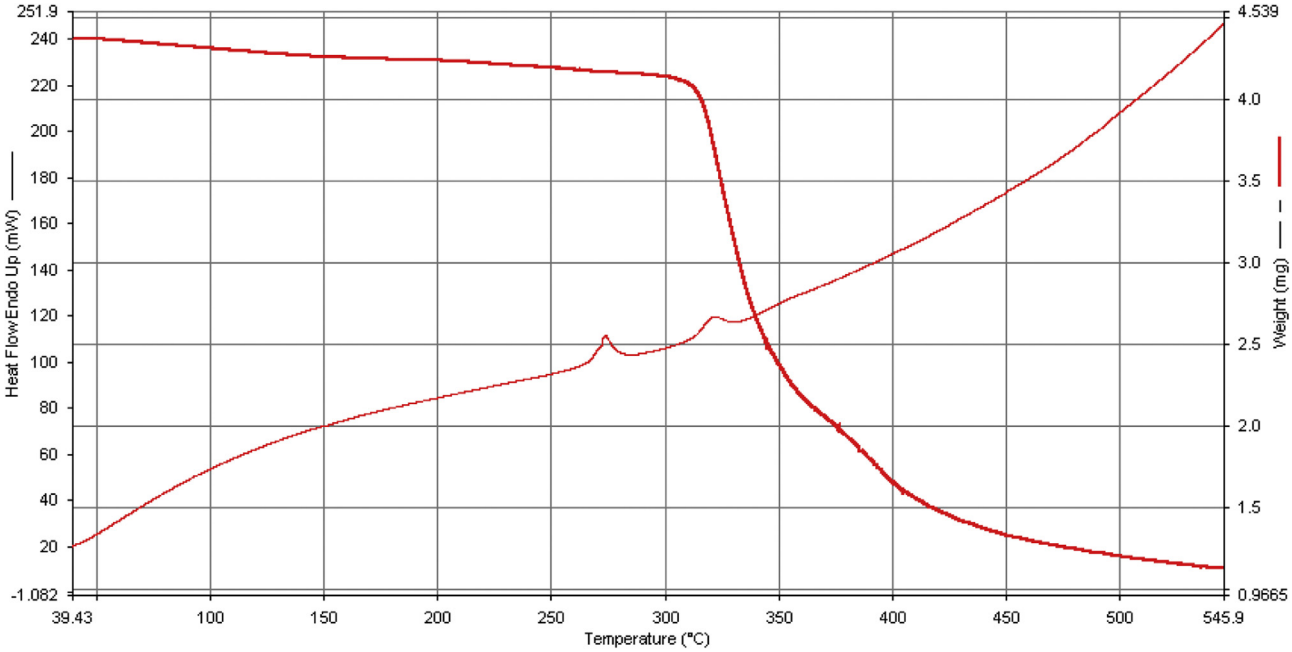

Fig. 7. TG curve of the compound (Heating rate 10 °C/min, Nitrogen atmosphere).

twist of the pyridyl moiety with respect to the imidazole moiety. The major share of interactions is due to **H···H** interactions which is 50.1% of total interactions. In **H···H** fingerprint plot the triangular shaped broad green region over blue background is again clustered around two regions. These are the close contact regions of H atoms to C atoms and N atoms due respectively to **C**—**H**···π interactions and **C**—**H**···**N** hydrogen bonding interactions. The **N**···**N** interactions correspond a negligible 0.1% of all atom-atom interactions in the crystal. Hirshfeld surface analysis thus clearly indicates that in the present crystal, directional assembly of **APIM** molecules is governed mainly by **C**—**H**···π and π···π interactions.

3.3. Results of DFT study

The minimum energy optimized structure of the **APIM** molecule has nearly the same bond lengths and bond angles (Table S1) as that has been observed in the crystal structures. The standard deviations of bond length and bond angles of **APIM** molecule between crystallographic and DFT computational results are 0.02 Å and 1.58° respectively (Table S2). The computed molecular dipole moment is nearly zero (0.0000005, 0.000000, 0.0000003) Debye. In the optimized geometry the pyridyl and the imidazole rings are also *trans* to each other like crystal structure. The dihedral angle

between the pyridyl and the imidazole ring plane in the optimized single molecule is 11.80° (which is 19.13° in crystal) (Fig. S1). Imidazolyl nitrogen (**N2**) and pyridyl nitrogen (**N3**) are rotate by 167.03° (crystal: 158.50°) with respect to each other. The linear extension of the ligand across two **N** atoms (**N2** and **N2***) of two imidazole ring is 11.69 Å (crystal: 11.754 Å). To assess the potentiality of **APIM** as a plausible ligand for metal chelation, we have attempted to estimate the rotational potential barrier across the connecting bond (**C3**–**C4**) between imidazole and pyridyl moiety. The DFT calculation reveals that this energy barrier is quite high (28.8072 kcal/mol) [Fig. S2]. This correlated well with fact that pyridyl forms intramolecular hydrogen bond (**C15**–**H15**···**N3**) with the central anthracene moiety of **APIM** which is also present in the crystal structure (Table S3). HOMO, LUMO, HOMO -1 and electrostatic potential (ESP) of the optimized structure have been depicted in Fig. 6. HOMO and LUMO both are mainly localized over the anthracene moiety whereas HOMO-1 is localized over the pyridyl imidazole part of the molecule. Highest negative charge concentration is over the pyridyl and imidazole **N**-atoms, whereas the hydrogen atoms attached to the bridging carbon atoms between central anthracene moiety and pyridyl-imidazole units are highest electro positive.

We have also optimized the **C**–**H**···π and π···π motifs starting with the similar initial geometry as has been observed in the crystal. These motifs also nicely converge to their respective minimum energy configuration. The **H** to (ring centroid) distance in the **C**–**H**···π optimized geometry is 3.116 Å (Fig. S3) and the centroid to centroid distance in the π···π motif is 3.874 Å (Fig. S4). The corrected binding energy for these motifs is 0.885 kcal/mole (for **C**–**H**···π) and 3.240 kcal/mol (for π···π). So the cohesive force generated the cooperative action **C**–**H**···π and π···π interaction can be approximated to be 4.125 kcal/mol.

3.4. Thermal-study

Thermal study of the molecular compound (Fig. 7) reveals a quite high decomposition temperature (320 °C) which is rarely seen in case of organic compounds. Starting from 50 °C up to 320 °C mass loss is very slow (~only 4.5%) and then within 350 °C 29% mass is lost. The mass loss behavior beyond 320 °C is more or less exponential in nature. One can clearly observe two small isotherms one at 275 °C and the other one at 330 °C. These clearly indicate the molecular rearrangement (phase change) within the solid. These two peaks can be assigned to two different intermolecular forces responsible for crystal packing – the **CH**···π and the π···π interactions. The separation between these peaks (~55 °C) indicates the differing strength of these interactions. The DFT study of intermolecular **CH**···π and π···π interactions reveal that **CH**···π interaction is stronger than π···π interactions in this system. One can estimate approximately the differing strength of these interactions to be ~k_BT = 55 k_B = 32.62 kcal/mol.

3.5. Photo physical study

Anthracene moiety is a well known fluorophore and the designing of the new molecular tecton utilizing anthracene at the core was with an aim to study the possible modulation of fluorescence property of the newly synthesized molecule. Fluorescence study of this molecule with various metal ions like Zn^{2+}, Co^{2+}, Ni^{2+},Mn^{2+},Fe^{2+},Al^{3+}, Tb^{2+} have been carried out. Experimental fluorescence spectra have been depicted in Fig. 8 and Figs. S5–S10. The general trend of the fluorescence spectra is a significant quenching of the fluorescence intensity of the 427 nm peak with the increase of metal ion concentration. Fig. 8 shows the change in the fluorescence intensity of anthracene emission at 450 nm in

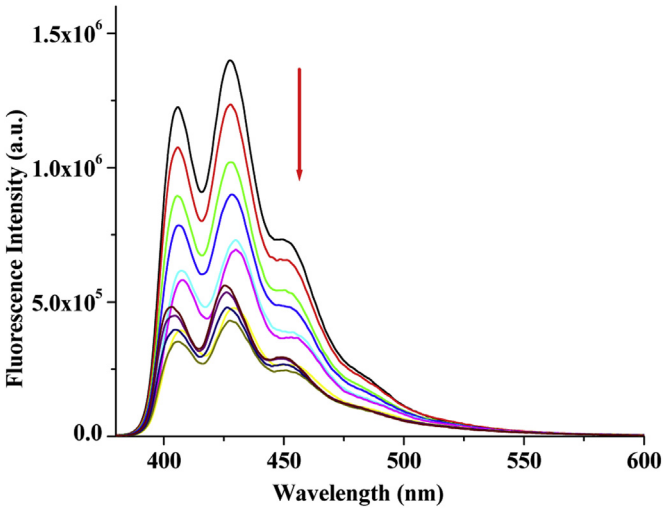

Fig. 8. Change in emission spectra of **APIM** (c = 2.5 × 10^{-5} M) upon addition of Zn^{2+} (c = 1.00 × 10^{-3} M, as perchlorate salt) in CH_3CN (λ_{ex} = 370 nm).

APIM in the presence of increasing amounts of Zn^{2+} ion concentration. A possible cause of quenching of fluorescence is that the molecule binds with the metal ions resulting a photo-induced electron transfer (PET) from the binding sites to the excited state of anthracene.

4. Conclusion

A new 2-(2′-Pyridyl)imidazole based symmetric organic molecule with anthracene fluorophore at its core has been synthesized. In the design of the molecule it was easy to foresee that π···π/**CH**···π interactions along with possible weak **CH**···**N** interaction could be possible cohesive forces for molecular self-assembly. Even in the presence of very few structure-directing interactions, predicting a crystal structure is a challenging task in crystal engineering [48] - so it was essential to obtain crystal structure to explore the specific manner in which π···π/**CH**···π forces operate in self-assembling **APIM**. The X-ray crystallographic analysis indeed revealed the simultaneous presence of both π···π/**CH**···π interactions in the molecular packing. The **Z**-shape of the molecule facilitates a rectangular assembly of two molecules through **CH**···π interaction having a calculated cohesion energy of 0.885 kcal/mole. Due to symmetric nature of the designed molecule with respect to the anthracene core this assembly self-propagates along the crystallographic ***b***-axis. It has often been observed that when more than one structure directing inter molecular forces are responsible for crystal packing, the forces generally propagates molecular assembly in mutually exclusive directions [49,50]. In a similar manner π···π interaction in the present crystal structure is responsible for molecular assembly along the crystallographic *a*-axis and **CH**···π interactions along crystallographic *b*-axis and thus both the interactions cooperate and coexist together in the present crystal. Successive supramolecular chains formed by **CH**···π interactions are further united into 2D supramolecular sheet by π···π interactions. The calculated π···π interaction energy of the molecule is 3.240 kcal/mol. Though the crystal has been assembled through weak forces only, it shows a moderately high thermal stability (320 °C) due to cooperative action of **CH**···π and π···π forces. The fluorescence study reveals that a series of metal ions act as efficient quencher for the fluorescence activity of the newly designed molecule. This new semi-rigid molecular tecton would possibly be an efficient ligand for metal coordination and might come out to be a good spacer for the design of porous and other functional

materials. Efforts towards this are currently underway in our laboratory.

Acknowledgements

This work is supported by the SERB-DST, New Delhi (Sanction No. SB/FT/CS-170/2012) and UGC Minor Research Project Grant (PSW-105/13-14(ERO)). A. D. Jana thanks UGC (New Delhi) for financial support under Minor Research Project, Grant no F.No.PSW-41/14-15 (ERO). Thanks to Prof. K. Ghosh, Department of Chemistry, University of Kalyani for using Fluorimeter in his DST funded project. We also thank Department of Chemistry, Assam University, Silchar, India, for providing us TG-DTA facility.

Appendix A. Supplementary data

Supplementary data associated with this article can be found in the online version, at http://dx.doi.org/10.1016/j.molstruc.2017.05.074. These data include MOL files and InChiKeys of the most important compounds described in this article.

References

[1] D.C. Sherrington, K.A. Taskinen, Self-assembly in synthetic macromolecular systems via multiple hydrogen bonding interactions, Chem. Soc. Rev. 30 (2001) 83–93, http://dx.doi.org/10.1039/b008033k.
[2] A.M. Beatty, Hydrogen bonded networks of coordination complexes, CrystEngComm 3 (2001) 243–255, http://dx.doi.org/10.1039/b109127c.
[3] C.B. Aakeröy, K.R. Seddon, The hydrogen bond and crystal engineering, Chem. Soc. Rev. 22 (1993) 397–407, http://dx.doi.org/10.1039/CS9932200397.
[4] A. Das, A.D. Jana, S.K. Seth, B. Dey, S.R. Choudhury, T. Kar, S. Mukhopadhyay, N.J. Singh, I. Hwang, K.S. Kim, Intriguing π + −π interaction in crystal packing, J. Phys. Chem. B 114 (2010) 4166–4170, http://dx.doi.org/10.1021/jp910129u.
[5] B.K. Mishra, N. Sathyamurthy, π-π Interaction in pyridine, J. Phys. Chem. A 109 (2005) 6–8, http://dx.doi.org/10.1021/jp045218c.
[6] C. Janiak, A critical account on π–π stacking in metal complexes with aromatic nitrogen-containing ligands †, J. Chem. Soc. Dalton Trans. (2000) 3885–3896, http://dx.doi.org/10.1039/b003010o.
[7] Y.-S. Liu, F.-B. Xu, J.-W. Wang, Q.-S. Li, H.-B. Song, Z.-Z. Zhang, 9,10-Bis[3-(2-pyridylmethyl)imidazolium-1-ylmethyl]anthracene bis(hexafluorophosphate), Acta Crystallogr. Sect. E. 61 (2005) o2930–o2931, http://dx.doi.org/10.1107/S1600536805023196.
[8] E.R.T. Tiekink, J. Zukerman-Schpector, Emerging supramolecular synthons: C–H•••π(chelate) interactions in metal bis(1,1-dithiolates), Chem. Commun. 47 (2011) 6623–6625, http://dx.doi.org/10.1039/c1cc11173f.
[9] Y. Kobayashi, K. Saigo, Periodic ab initio approach for the cooperative effect of CH/π interaction in crystals: relative energy of CH/π and hydrogen-bonding interactions, J. Am. Chem. Soc. 127 (2005) 15054–15060, http://dx.doi.org/10.1021/ja0434580.
[10] J.L. Ferguson, C.M. Fitchett, N,N′-dimethylene-2,2′-biimidazole-a mimic of carboxylate for the formation of complexes with copper(I) and the anion directed formation of a solvent pocket, Cryst. Growth Des. 15 (2015) 1280–1288, http://dx.doi.org/10.1021/cg5016803.
[11] E.C. Yang, Y.N. Chan, H. Liu, Z.C. Wang, X.J. Zhao, Unusual polymeric Zn (II)/Cd (II) complexes with 2,6-diaminopurine by synergistic coordination of nucleobases and polycarboxylate anions: binding behavior, self-assembled pattern of the nucleobase, and luminescent properties, Cryst. Growth Des. 9 (2009) 4933–4944, http://dx.doi.org/10.1021/cg9007119.
[12] M. Bagherzadeh, L. Tahsini, R. Latifi, A. Ellern, L.K. Woo, Synthesis, crystal structure and catalytic activity of a novel Mo(VI)-oxazoline complex in highly efficient oxidation of sulfides to sulfoxides by urea hydrogen peroxide, Inorganica Chim. Acta 361 (2008) 2019–2024, http://dx.doi.org/10.1016/j.ica.2007.10.017.
[13] O.R. Evans, W. Lin, Crystal engineering of NLO materials based on metal-organic coordination networks, Acc. Chem. Res. 35 (2002) 511–522, http://dx.doi.org/10.1021/ar0001012.
[14] T.B. Hughes, G.P. Miller, S.J. Swamidass, Site of reactivity models predict molecular reactivity of diverse chemicals with glutathione, Chem. Res. Toxicol. 28 (2015) 797–809, http://dx.doi.org/10.1021/acs.chemrestox.5b00017.
[15] M. Khatua, P.K. Chattaraj, Molecular reactivity dynamics in a confined environment, Phys. Chem. Chem. Phys. 15 (2013) 5588, http://dx.doi.org/10.1039/c3cp43511c.
[16] D.N. Dybtsev, H. Chun, K. Kim, Rigid and flexible: a highly porous metal–organic framework with unusual guest-dependent dynamic behavior, Angew. Chem. 116 (2004) 5143–5146, http://dx.doi.org/10.1002/ange.200460712.
[17] P.-Q. Liao, D.-D. Zhou, A.-X. Zhu, L. Jiang, R.-B. Lin, J.-P. Zhang, X.-M. Chen, Strong and dynamic CO 2 sorption in a flexible porous framework possessing guest chelating claws, J. Am. Chem. Soc. 134 (2012) 17380–17383, http://dx.doi.org/10.1021/ja3073512.
[18] B. Manna, A.K. Chaudhari, B. Joarder, A. Karmakar, S.K. Ghosh, Dynamic structural behavior and anion-responsive tunable luminescence of a flexible cationic metal-organic framework, Angew. Chem. - Int. Ed. 52 (2013) 998–1002, http://dx.doi.org/10.1002/anie.201206724.
[19] A.K. Ghosh, A.D. Jana, D. Ghoshal, G. Mostafa, N.R. Chaudhuri, Toward the recognition of enolates/dicarboxylates: syntheses and X-ray crystal structures of supramolecular architectures of Zn(II)/Cd(II) Using 2,2'-biimidazole, Cryst. Growth Des. 6 (2006) 701–707, http://dx.doi.org/10.1021/cg050473n.
[20] C. Borel, K. Larsson, M. Håkansson, B.E. Olsson, A.D. Bond, L. Öhrström, Oxalate- and squarate-biimidazole supramolecular synthons: hydrogen-bonded networks based on [Co(H2biimidazole)3]3+, Cryst. Growth Des. 9 (2009) 2821–2827, http://dx.doi.org/10.1021/cg900075j.
[21] S. Rui-Li, X. Li, Supramolecular architectures of cadmium(II) built of 2,2′-biimmidazole and bifunctional carboxylates: syntheses, crystal structure and properties, Inorganica Chim. Acta 359 (2006) 525–532, http://dx.doi.org/10.1016/j.ica.2005.09.039.
[22] K.D. Benkstein, J.T. Hupp, C.L. Stern, Synthesis and characterization of molecular rectangles based upon rhenium thiolate dimers, Inorg. Chem. 37 (1998) 5404–5405, http://dx.doi.org/10.1021/IC980513V.
[23] F.E. Hahn, C. Radloff, T. Pape, A. Hepp, A nickel(II) -cornered molecular rectangle with biscarbene and 4,4′-bipyridine bridging groups, Organometallics 27 (2008) 6408–6410, http://dx.doi.org/10.1021/om801007u.
[24] M.L. Yen, N.C. Chen, C.C. Lai, Y.H. Liu, S.M. Peng, S.H. Chiu, A molecular cage that selectively complexes three different guests in solution, Org. Lett. 11 (2009) 4604–4607, http://dx.doi.org/10.1021/ol901873m.
[25] R. McCaffrey, H. Long, Y. Jin, A. Sanders, W. Park, W. Zhang, Template synthesis of gold nanoparticles with an organic molecular cage, J. Am. Chem. Soc. 136 (2014) 1782–1785, http://dx.doi.org/10.1021/ja412606t.
[26] V. Stavila, A.A. Talin, M.D. Allendorf, MOF-based electronic and opto-electronic devices, Chem. Soc. Rev. 43 (2014) 5994–6010, http://dx.doi.org/10.1039/C4CS00096J.
[27] Q.-Y. Xiang, K. Zhang, Y. Wang, X.-J. Lou, W.-Q. Yao, Y. Bai, D.-W. Duan, X.-P. Hu, J. Wang, Z.-D. Luo, H.-H. Wang, L.-X. Zhang, U. Klemradt, J.-L. Cao, Insight into metalized interfaces in nano devices by surface analytical techniques, ACS Appl. Mater. Interfaces 7 (2015) 27351–27356, http://dx.doi.org/10.1021/acsami.5b08919.
[28] Y. Cui, Y. Yue, G. Qian, B. Chen, Luminescent functional metal–organic frameworks, Chem. Rev. 112 (2012) 1126–1162, http://dx.doi.org/10.1021/cr200101d.
[29] M.D. Allendorf, C.A. Bauer, R.K. Bhakta, R.J.T. Houk, Luminescent metal–organic frameworks, Chem. Soc. Rev. 38 (2009) 1330, http://dx.doi.org/10.1039/b802352m.
[30] P. Suresh, A. Samanta, A. Sathyanarayana, G. Prabusankar, Synthesis and characterization of vinylimidazolium salts : solution state study to realize the influence of different anions, J. Mol. Struct. 1024 (2012) 170–175, http://dx.doi.org/10.1016/j.molstruc.2012.05.030.
[31] K. Biradha, M. Sarkar, L. Rajput, Crystal engineering of coordination polymers using 4,4′-bipyridine as a bond between transition metal atoms, Chem. Commun. (2006) 4169–4179, http://dx.doi.org/10.1039/B606184B.
[32] R.D. Hancock, The pyridyl group in ligand design for selective metal ion complexation and sensing, Chem. Soc. Rev. 42 (2013) 1500–1524, http://dx.doi.org/10.1039/C2CS35224A.
[33] S.-S. Chen, The roles of imidazole ligands in coordination supramolecular systems, CrystEngComm 18 (2016) 6543–6565, http://dx.doi.org/10.1039/C6CE01258B.
[34] H. Motegi, L. Hu, C. Slebodnick, B.E. Hanson, Microporous and mesoporous materials synthesis and structure of two novel cobalt (II) and zinc (II) crystalline coordination networks constructed with 1, 3, 5-benzene tricarboxylate and 9, 10-bis (imidazol-1-ylmethyl) anthracene, Microporous Mesoporous Mater 129 (2010) 360–365, http://dx.doi.org/10.1016/j.micromeso.2009.06.009.
[35] W. Kan, J. Yang, Y. Liu, J. Ma, A series of metal – organic frameworks based on 9, 10-bis (imidazol-1-ylmethyl) anthracene and structurally related aromatic dicarboxylates : syntheses, structures, and photoluminescence, Polyhedron 30 (2011) 2106–2113, http://dx.doi.org/10.1016/j.poly.2011.05.035.
[36] G. Stupka, L. Gremaud, A.F. Williams, Control of redox potential by deprotonation of coordinated 1H-imidazole in complexes of 2-(1H-imidazol-2-yl) pyridine, Helv. Chim. Acta 88 (2005) 487–495, http://dx.doi.org/10.1002/hlca.200590033.
[37] S.M. Yue, H. Bin Xu, J.F. Ma, Z.M. Su, Y.H. Kan, H.J. Zhang, Design and syntheses of blue luminescent zinc(II) and cadmium(II) complexes with bidentate or tridentate pyridyl-imidazole ligands, Polyhedron 25 (2006) 635–644, http://dx.doi.org/10.1016/j.poly.2005.07.021.
[38] W. Liu, Y. Wang, M. Sun, D. Zhang, M. Zheng, W. Yang, Alkoxy-position effects on piezofluorochromism and aggregation-induced emission of 9,10-bis(alkoxystyryl)anthracenes, Chem. Commun. 49 (2013) 6042, http://dx.doi.org/10.1039/c3cc42636j.
[39] H. Wang, Y. Liu, M. Li, H. Huang, H.M. Xu, R.J. Hong, H. Shen, Multifunctional TiO2 nanowires-modified nanoparticles bilayer film for 3D dye-sensitized solar cells, Optoelectron. Adv. Mater. Rapid Commun. 4 (2010) 1166–1169, http://dx.doi.org/10.1039/b000000x.
[40] G.M. Sheldrick, Crystal structure refinement with SHELXL, Acta Crystallogr. Sect. C Struct. Chem. 71 (2015) 3–8, http://dx.doi.org/10.1107/

S2053229614024218.
[41] M.A. Spackman, J.J. McKinnon, Fingerprinting intermolecular interactions in molecular crystals, CrystEngComm 4 (2002) 378–392, http://dx.doi.org/10.1039/B203191B.
[42] P.A. Wood, J.J. McKinnon, S. Parsons, E. Pidcock, M.A. Spackman, Analysis of the compression of molecular crystal structures using Hirshfeld surfaces, CrystEngComm 10 (2008) 368–376, http://dx.doi.org/10.1039/b715494a.
[43] J.J. McKinnon, A.S. Mitchell, M.A. Spackman, Hirshfeld surfaces: a new tool for visualising and exploring molecular crystals, Chem. - A Eur. J. 4 (1998) 2136–2141, http://dx.doi.org/10.1002/(SICI)1521-3765(19981102)4:11<2136::AID-CHEM2136>3.0.CO;2-G.
[44] A.L. Rohl, M. Moret, W. Kaminsky, K. Claborn, J.J. McKinnon, B. Kahr, Hirshfeld surfaces identify inadequacies in computations of intermolecular interactions in crystals: pentamorphic 1,8-dihydroxyanthraquinone, Cryst. Growth Des. 8 (2008) 4517–4525, http://dx.doi.org/10.1021/cg8005212.
[45] S.K. Seth, D. Sarkar, A.D. Jana, T. Kar, On the possibility of tuning molecular edges to direct supramolecular self-assembly in coumarin derivatives through cooperative weak forces: crystallographic and hirshfeld surface analyses, Cryst. Growth Des. 11 (2011) 4837–4849, http://dx.doi.org/10.1021/cg2006343.
[46] S.K. Wolff, D.J. Grimwood, J.J. McKinnon, D. Jayatilaka, M.A. Spackman, Crystal Explorer 2.0, (n.d.).
[47] J.A.P.M.J. Frisch, G.W. Trucks, H.B. Schlegel, G.E. Scuseria, M.A. Robb, J.R. Cheeseman, J.A. Montgomery, T. Vreven, K.N. Kudin, J.C. Burant, J.M. Millam, S.S. Iyengar, J. Tomasi, V. Barone, B. Mennucci, M. Cossi, G. Scalmani, N. Rega, G.A. Petersso, Gaussian 03 Package, 2003.
[48] G.R. Desiraju, Crystal engineering: a holistic view, Angew. Chem. - Int. Ed. 46 (2007) 8342–8356, http://dx.doi.org/10.1002/anie.200700534.
[49] B. Dey, S.R. Choudhury, E. Suresh, A.D. Jana, S. Mukhopadhyay, Use of π•••π forces to steer the assembly of a NTA complex of Cu(II) into hydrogen bonded supramolecular layers (H_3NTA=nitrilotriacetic acid), J. Mol. Struct. 921 (2009) 268–273, http://dx.doi.org/10.1016/j.molstruc.2009.01.004.
[50] S.R. Choudhury, H.M. Lee, T.-H. Hsiao, E. Colacio, A.D. Jana, S. Mukhopadhyay, Co-operation of π•••π, Cu(II)•••π, carbonyl•••π and hydrogen-bonding forces leading to the formation of water cluster mimics observed in the reassessed crystal structure of [Cu(mal)(phen)(H_2O)]$_2\cdot 3H_2O$ (H_2mal=malonic acid, phen=1,10-phenanthroline), J. Mol. Struct. 967 (2010) 131–139, http://dx.doi.org/10.1016/j.molstruc.2009.12.048.